Research Article | Vol. 27, No. 11 | 27 May 2019 | OPTICS EXPRESS 16405
Optics EXPRESS

Multi-octave visible to long-wave IR femtosecond continuum generated in Cr:ZnS-GaSe tandem

SERGEY VASILYEV,[1,*] IGOR MOSKALEV,[1] VIKTOR SMOLSKI,[1] JEREMY PEPPERS,[1] MIKE MIROV,[1] ANDREY MURAVIEV,[3] KONSTANTIN VODOPYANOV,[3] SERGEY MIROV,[1,4] AND VALENTIN GAPONTSEV[2]

[1]*IPG Photonics – Southeast Technology Center, 100 Lucerne Ln., Birmingham, AL 35211, USA*
[2]*IPG Photonics Corporation, 50 Old Webster Rd, Oxford, MA 01540, USA*
[3]*CREOL, College of Optics and Photonics, Univ. Cent. Florida, Orlando, FL 32816, USA*
[4]*Department of Physics, University of Alabama at Birmingham, 1530 3rd Ave S, Birmingham AL 35294, USA*
**svasilyev@ipgphotonics.com*

Abstract: We report a technique for generation of broad and coherent femtosecond (fs) continua that span several octaves from visible to long-wave IR parts of the spectrum (0.4–18 μm). The approach is based on simultaneous amplification of few-cycle pulses at 2.5 μm central wavelength at 80 MHz repetition rate, and augmentation of their spectrum via three-wave mixing in a tandem arrangement of polycrystalline Cr:ZnS and single crystal GaSe. The obtained average power levels include several mW in the 0.4–0.8 μm visible, 0.23 W in the 0.8–2 μm near-IR, up to 4 W in the 2–3 μm IR, and about 17 mW in the 3–18 μm long-wave IR bands, respectively. High brightness and mutual coherence of all parts of the continuum was confirmed by direct detections of the carrier envelope offset frequency of the master oscillator.

1. Introduction

Ultra-broadband laser-like sources with high spatial and temporal coherence are in great demand for a large number of applications that range from imaging and spectroscopy [1–3] to massively-parallel real-time fingerprinting of molecules [4,5]. Coherent multi-octave continua are also essential for arbitrary multi-color optical waveform synthesis [6,7].

The standard approach to generation of multi-octave spectra is based on supercontinuum generation (SCG) in fibers [8–10], waveguides [11,12], and bulk media [13,14]. All these techniques yield broad spectral spans, including the demonstrations of ultra-broad SC extending from the UV into the middle IR (MIR) that were achieved in hollow-core fibers and in bulk. Experimental implementations of bulk multi-octave SCG are very straightforward but they require sophisticated MIR pump laser systems with high (multi-μJ) pulse energy that operate at low, typically kHz, repetition rates. Solid-core fibers and waveguides enable SCG at full multi-MHz repetition rates of the mode-locked oscillators. However, the solid core geometries have intrinsic power limitations and alignment sensitivity issues.

SCG can also be enabled by second order nonlinearity of the medium. Broad continua were obtained via cascaded quadratic nonlinearities (CQN) in bulk and in guiding $\chi^{(2)}$ devices [15–18]. It has been demonstrated [19,20] that CQN induces an effective nonlinear index $n_{2,CQN}$. Thus, the CQN enables an engineering of the nonlinear propagation of fs pulses by the control of the sign and the strength of self-phase modulation (SPM) and of the effective Kerr lens [21]. More recently, multi-octave continua were generated in bulk polycrystalline ZnSe

#358470 https://doi.org/10.1364/OE.27.016405
Journal © 2019 Received 28 Jan 2019; revised 15 May 2019; accepted 15 May 2019; published 24 May 2019

Optics EXPRESS

pumped at kHz repetition rate by radiation of optical parametric amplifiers [22,23]. The authors of [22] interpreted their results as harmonics-enhanced supercontinuum generation.

In this paper we present an approach to generation of multi-octave continua that is based on a tandem of two highly nonlinear materials: Cr:ZnS and GaSe, with the former serving simultaneously as a laser gain material. Via a chain of three-wave mixings we obtain a set of five mutually coherent comb-like spectra. The all-bulk architecture is compatible with low pulse energies (from nJ to sub-μJ levels) and supports high pulse repetition frequencies and high, multi-Watt average power.

The approach is based on the results of two recent experiments [24,25]. In [24] we reported a three-octave (0.4–3.4 μm) spectrum generated by sum-frequency mixing of super-octave fs pulses centered at 2.5 μm. The second paper reported the generation of long wave IR (LWIR) transients in the range 4.3–17.6 μm via intrapulse difference-frequency generation (IDFG), which was driven by a 6 W sub-octave 2.5 μm fs source. Here we bridge the gap and obtain a continuous coherent spectrum that spans all the way from the visible (VIS) to the LWIR. Thus, we combine harmonics-enhanced SCG, which occurs at full repetition rate of a fs oscillator, with a new regime of optical rectification where the spectrum of MIR input pulses completely merges with the spectrum of generated LWIR transients. The latter result can be interpreted as supercontinuum generation augmented by optical rectification.

2. Experimental setup

The schematic of the laser setup is shown in Fig. 1. We first reproduced an octave spanning laser system from [24]. This part of the setup is encircled in Fig. 1 with a dashed rectangle. The key components of the laser are: (i) a 3-cycle master oscillator at 2.4 μm central wavelength with 1.1 W average power at pulse repetition frequency f_R = 78 MHz and (ii) a single-pass amplifier-&-nonlinear converter. Both the oscillator and the amplifier are based on polycrystalline Cr:ZnS and are optically pumped by radiation of commercial Er-doped fiber lasers (EDFLs), and are cooled with room temperature water. Seed pulses from the oscillator are superimposed with EDFL radiation on a dispersive mirror (M*) and coupled to the amplifier at full repetition rate. Amplified pulses at the fundamental wavelength are separated by a pair of broadband dichroic mirrors (DM).

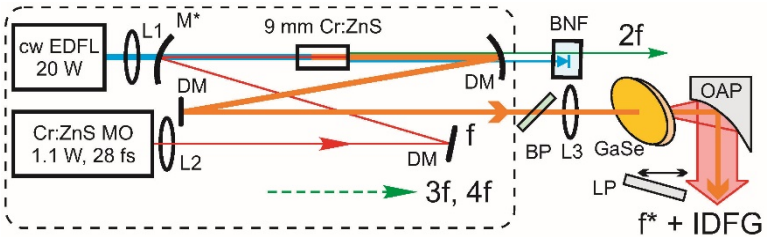

Fig. 1. Experimental setup. MO, master oscillator; EDFL, pump laser for the single-pass Cr:ZnS amplifier-&-nonlinear converter; L1–3, AR-coated plano-convex lenses (focal lengths 80, 750, 20 mm, respectively); M*, DM dichroic mirrors (see main text and Ref [24].). The main MIR signal (f) is separated from second harmonic (2f) by mirrors DM. The residual pump radiation in 2f-output is suppressed by an OptiGrate Bragg notch filter (BNF). Higher optical harmonics (3f, 4f) are accessed via residual signal in the main f-output. GaSe sample is installed on a 5-axis stage (see main text and Ref [25].); a 4 mm thick YAG Brewster plate (BP) is used for inter-stage dispersion control. IDFG signal and augmented main signal (f*) are collimated by gold-coated 90° off-axis parabola with RFL = 25.4 mm (OAP); spectral components are separated by a set of long-pass filters (LP).

The single-pass amplifier was equipped with off-the-shelf 9 mm long polycrystalline Cr:ZnS gain element ($6.3 \cdot 10^{-18}$ cm^{-3} Cr^{2+} concentration, $0.72 \cdot 10^{18}$ cm^2 absorption cross-section at the pump wavelength 1567 nm, 2% low-signal pump transmission and 40 kW pump saturation intensity). The average size of the grain in the gain element was about 30 μm, which approximately equals the coherence length of 2400 nm → 1200 nm second

Optics EXPRESS

harmonic generation (SHG). The amplifier was optimized for maximum spectral broadening of seed pulses. The optimizations were carried out experimentally [24], including pre-chirping of input pulses (with group delay dispersion GDD ≈800 fs^2) and fine-tuning of the transverse size of the seed beam (≈170 μm $1/e^2$ intensity diameter in the gain element).

After propagating through the optimized single-pass amplifier, the seed pulses are amplified to 4.2 W, their spectrum is broadened to an optical octave, and the pulse duration is reduced to about 2 cycles. Further, the MIR spectrum is converted to a three-octave continuum via sum-frequency mixing directly in the Cr:ZnS element. We utilized to full extent the unique combination of laser, nonlinear-optical, and physical properties of polycrystalline Cr:ZnS: (i) this laser material allows for direct generation and amplification of few-cycle optical pulses [26,27]; (ii) ZnS is a semiconductor with high 2nd and 3rd order nonlinearities (d_{36} ≈6 pm/V, n_2 ≈10^{-15} cm^2/W at the wavelength of 2.5 μm [22],); (iii) polycrystalline microstructure enables random quasi phase matching (RQPM) with ultra-broad bandwidth [28]. Thus, propagation of MIR fs pulses through polycrystalline Cr:ZnS is simultaneously governed by laser interactions, three-wave mixings between the different spectral components within the same pulse, and SPM and self-focusing (self-defocusing [21],) that arise from $\chi^{(3)}$ as well as from the effective nonlinear index $n_{2,CQN}$.

The spectrum of an entire 0.4–4 μm continuum was characterized in [24]. For the purposes of the present study we separated the fundamental MIR band from the NIR second harmonic (shown in Fig. 1 as f- and 2f-outputs, respectively). The residual pump radiation in the 2f-output was suppressed by a high performance notch filter provided by OptiGrate. We utilized the residual 3f-4f signal in the main f-output to confirm continuity and coherence of the spectrum down to the visible wavelengths, as will be discussed in the next section.

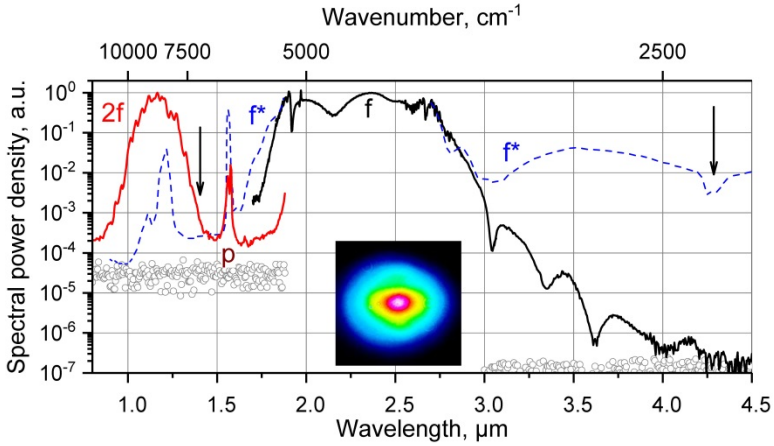

Fig. 2. Spectra of pulses in f (black) and 2f (red) outputs of the Cr:ZnS laser (presented in log scale, both peaks are normalized to unity). The central part of the f-peak was acquired by a Thorlabs OSA207C. The wing of the f-peak was acquired with higher dynamic range by an Acton monochromator with a 150 g/mm grating, LP 2.5 μm filter, and a Teledyne J14 MCT detector (LN cooled). The spectra were then stitched together. The 2f-peak was acquired with the same monochromator and a Thorlabs InGaAs DET10D detector. Scattered dots show the noise floors. Dashed lines show the wings of the augmented main signal (f*) after propagation trough the GaSe sample (see main text). Peaks (p) at 1.567 μm correspond to residual cw signals of EDFL pump. Vertical arrows show the wavelengths of f_{CEO} measurements. The inset shows the profile of the main output beam at 4.2 W power (taken by DataRay IR camera).

Spectra of pulses, which were measured at f- and 2f-outputs of the Cr:ZnS source are represented in Fig. 2 by solid lines. The fundamental MIR spectrum is truncated due to the limited bandwidth of the DMs. We measured 4.2 W average power in fundamental MIR band, which corresponds to 54 nJ pulse energy at 78 MHz repetition rate. We conservatively estimate 19 fs MIR pulse duration and 2.5 MW peak power (see discussion in [24,25]). The

Optics EXPRESS

NIR part of the continuum at second harmonic wavelength has 0.23 W average power. The measured spectrum of pulses at 2f output confirms ultra-wide bandwidth of the RQPM process: f and 2f pulses feature similar bandwidths (about 60 THz at 10 dB level with respect to the main peaks). Significant group velocity mismatch between f and 2f signals (about 170 fs/mm) results in temporal broadening of SHG pulses to few hundred fs [28]. The average power of the combined 3f and 4f signals was at few-mW level.

The MIR output of the Cr:ZnS source was fed to the second stage of the tandem that comprised a GaSe crystal configured for IDFG, as described in [23]. Important limitation on the efficiency of IDFG process (which is equivalent to optical rectification) arises from the group velocity mismatch between driving pulses and generated transients. In our case of 2-cycle MIR driving pulses at central wavelength 2.5 μm, the effective interaction length L_{eff} ≈1.5 mm [29], which approximately equals the thickness of our GaSe sample (L_{GaSe} = 1 mm). In contrast to our previous report [25], we did not follow the standard design considerations from [29] and optimized the IDFG stage for broadest spectrum of output pulses. We used a monochromator and a long-pass filter (LP) to simultaneously monitor the optical signal at 4.5 μm (i.e. in the region of the overlap between the fundamental and IDFG spectra) and measure overall IDFG output power at wavelengths above 6.7 μm. The optimizations included selection of the focal length of the lens L3, location of the GaSe sample along the focus, orientation of the sample, and selection of the thickness of the dispersion-control plate (BP). As a result of optimizations, the driving pulses were over-focused to a spot size of about 30 μm vs. 150 μm spot that was used in [25] ($1/e^2$ intensity diameter in both cases).

3. Results and discussion

Spectral parameters of the optimized setup are illustrated in Fig. 3. The part of the spectrum at wavelengths above 3 μm is shown in Fig. 3(a) in linear scale. As can be seen, the optical signal at 4.5 μm wavelength is 10% of that of the central IDFG peak at 7 μm. This is a two orders of magnitude improvement over that previously reported [25]. We discovered that the strength of the signal in the region of spectral overlap is sensitive to the location and orientation of the GaSe sample. For instance, the spectrum in Fig. 3(a) corresponds to the displacement of the sample along the beam, away from the focal point (by a fraction of mm) and a minor change of the phase-matching angle θ with respect to the IDFG optimum. Even stronger optical signals in the 4.5 μm band can be obtained at the expense of the overall power of the IDFG signal. Thus, Fig. 3(a) corresponds to a compromise between the spectral power density at 4.5 μm and the total optical power of IDFG signal.

We also observed a significant broadening in the region of the initial laser spectrum near 2.5 μm after their propagation through the GaSe sample. Dashed lines in Fig. 2 show the measured optical signals in the long-wave and in the short-wave wings of the main spectral peak after the interaction with GaSe. As can be seen, the red-shifted spectral components appear at very significant levels with respect to the main peak (as high as −14 dB) while the blue-shifted components appear at about −30 dB level. The red-shift of fs pulses due to IDFG process and the related cascading effects were predicted [29] and then observed [30] in the context of generation of THz transients. In short, difference frequency mixing between driving pulses (central frequency ν_0) and the IDFG transients ($\nu_{IDFG} < \nu_0$) results in appearance of new spectral components at intermediate frequencies $\nu_{IDFG} < \nu^* < \nu_0$. The new spectral components ν^* also participate in IDFG processes producing new components in IDFG spectrum ν^*_{IDFG}, there $\nu_{IDFG} < \nu^*_{IDFG} < \nu^*$. All of the above difference frequency mixings result in decays of “blue” photons from the high-frequency part of the spectrum into pairs of low-frequency photons. Thus the whole spectrum experiences a red-shift.

Optics EXPRESS

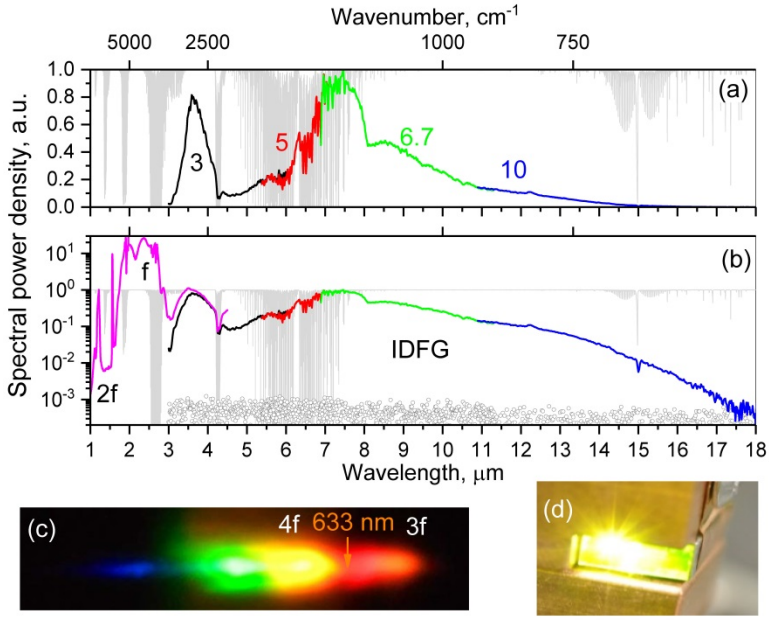

Fig. 3. Overall spectrum of the continuum. (a) part of the spectrum in linear scale acquired by an Acton monochromator with a 75 g/mm grating, a Teledyne J22 MCT detector (LN cooled), and a set of LPs with 3, 5, 6.7, 10 μm cut-on. Obtained data were normalized to LP transmission and stitched (as shown by different colors). (b), the same spectra are presented in log scale and combined with the high power part of the continuum from Fig. 2. The curves somewhat mismatch because IDFG and f spectra were acquired in different experiments, using different gratings, detectors, and filters. (c), VIS (4f) and NIR (3f) part of the continuum dispersed by a prism (vertical arrow shows the approximate wavelength of the f_{CEO} measurement). (d), a photo of polycrystalline Cr:ZnS during the laser operation.

Our experiments reveal similar effects but on a significantly larger scale, in terms of spectral coverage. This can be explained by (i) extremely broad spectrum of the input pump pulses and (ii) higher tolerance of the three-wave interactions for detuning due to the smaller difference in the photon energies, as compared to THz generation. In essence, we reproduce the classical experiments with Ti:sapphire oscillators [31–33]. In our case, the spectrum of few-cycle MIR driving pulses merges with the spectrum of offset-free LWIR transients, but with less complex experimental arrangement. Further, the distribution of the optical power in the resultant spectrum can be fine-tuned by the adjustment of the angular phase-matching conditions. We also acknowledge two very recent publications on similar topics [34,35].

Optics EXPRESS

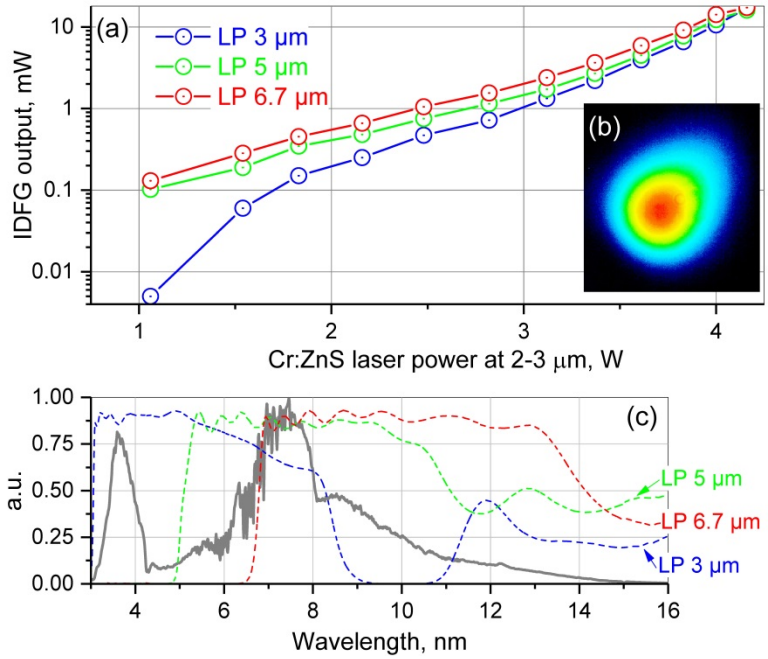

Fig. 4. (a) Measured IDFG output power vs. input power at fundamental wavelength measured behind LPs with 3, 5, 6.7 μm cut-on wavelength and presented in log scale. (b) IDFG beam profile measured behind LP 6.7 μm at the maximum 17 mW power. (c) Normalized spectrum of IDFG signal from Fig. 3(a) (shown by grey color) is compared with measured transmissions of LPs with 3, 5, 6.7 μm cut-on wavelength (shown by blue, green, and red colors, respectively).

The overall IR spectrum of the Cr:ZnSe-GaSe tandem is shown in Fig. 3(b) and 3(c). In Fig. 3(b) we stitched together the spectrum of augmented driving pulses with the spectrum from Fig. 3(a) and presented the result in logarithmic scale (we measured 2.5 W laser power behind the GaSe sample). Measured spectra of the visible and the near-IR parts of the continuum (4f and 3f signals, respectively) are provided in [24]. Here we dispersed the residual 4f-3f signal in the main laser beam with a prism and took the photo shown in Fig. 3(c). A photo of polycrystalline Cr:ZnS amplifier gain element in action is shown in Fig. 3(d).

The achievable power levels in the important 3–18 μm IR band are shown in Fig. 4. We measured the average power of IDFG signal behind 3, 5, and 6.7 μm LPs vs. input power from the Cr:ZnS laser. LWIR power as high as 17 mW was measured at the maximum 4.2 W input power. This corresponds to 0.4% power conversion. Our long-pass filters have limited bandwidth and introduce significant losses, as illustrated in Fig. 4(c). Therefore, one can estimate 20 mW LWIR power and 0.5% efficiency in the setup with optimized wavelength separation. Figure 4 also illustrates highly nonlinear dependences of the LWIR signals on the applied Cr:ZnS laser power, which was also discussed in [25]. We explain very high (stronger than quadratic) steepness of the dependences by an onset of self-focusing of driving pulses in the GaSe sample. Indeed, 2.5 MW peak power of driving pulses significantly exceeds the critical power for self-focusing in GaSe as $P/P_{Crit} \approx 16 >> 1$ (here we assume the nonlinear index $n_2 = 2 \cdot 10^{-14}$ cm^2/W). Tight focusing of driving pulses in the sample results in a short characteristic self-focusing distance of $z_{sf} \approx 0.3$ mm $< L_{GaSe}$ (here we use the formulae from [36]). Thus, an increase of input power results in significant and nonlinear increase of optical intensity over the length of the sample. In our previous experiment [25] the focusing was loose ($z_{sf} \approx 6$ mm $>> L_{GaSe}$) and hence the effects due to self-focusing were less pronounced.

Optics EXPRESS

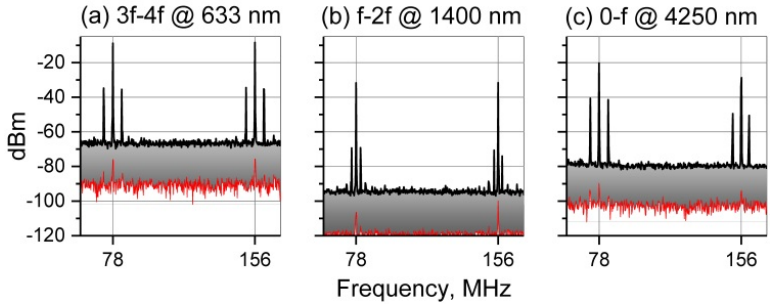

Fig. 5. RF spectra of interference beatings between the adjacent comb-like spectra measured in a 10 kHz resolution bandwidth (a Rohde & Schwarz FSEA RF spectrum analyzer) (a) a Thorlabs FL632.8-3 filter and Si APD430A detector, (b) a Thorlabs FB1400-12 filter and an InGaAs New Focus 1611 receiver, (c) a Spectrogon BP4260-150 filter and an InSb Kolmar KISDP-0.1 detector (LN cooled). Measurements were carried out in the course of 2 weeks at the same laser setpoint. Different measured values of the f_{CEO} are likely due to the fluctuations of the environment (temperature in the lab, residual humidity in the laser compartment).

The obtained multi-octave spectrum represents a superposition of several comb-like spectra with the same mode spacing f_R = 78 MHz but different offsets. By the nature of IDFG, the offset of the LWIR comb equals zero, while the offsets of the optical harmonics equal $n \cdot f_{CEO}$, where n is the harmonic order and f_{CEO} is the carrier envelope offset frequency of the master oscillator. Thus, any pair of adjacent combs must beat at the same f_{CEO}. We used this feature to prove the coherence, low intensity fluctuations, and high brightness of the frequency continua by measuring 3f-4f, f-2f, 0-f interference beatings at 0.633 μm, 1.4 μm, and 4.25 μm wavelengths using off-the-shelf band-pass filters and photodetectors (2f-3f beating was reported in [24]). Spectra of detected rf signals are presented in Fig. 5. All three rf spectra reveal strong f_{CEO} sidebands with the strongest beats (40 dB above the noise level) achieved in the MIR (at 4.25 μm, Fig. 5(c)). Relatively weak f-2f beating in the NIR (at 1.4 μm, Fig. 5(b)) can be explained by large spatiotemporal mismatches in this optical band.

4. Conclusion

We developed an approach to generation of exceptionally broad continua that span from the visible to the LWIR. We confirmed the coherence of the generated continuum by observation of the interference beatings between the adjacent comb-like spectra. The all-bulk single-pass Cr:ZnS-GaSe tandem architecture is robust, simple to implement, and supports high pulse repetition rates and high average powers. Achieved 17 mW power in the important offset-free 0-f LWIR part of the continuum is sufficient for a number of applications related to molecular spectroscopy, including various dual frequency comb techniques [4,5,37]. Sub-Watt power level in the 2f NIR part of the continuum provides possibilities for referencing and stabilization of the whole set of comb-like modes to low-noise ultra-narrowband lasers, which are readily available (e.g. near 1 μm wavelength). Significant optical power density in the 3f-4f VIS part of the continuum enables measurement of the f_{CEO} of the MIR oscillator with low-cost Si detectors. This f_{CEO} measurement scheme does not require any alignment and is insensitive to the external noise. Thus, we can measure (and, hence, stabilize) the f_{CEO} of a Cr:ZnS oscillator as straightforwardly as its repetition rate f_R. Directions of further research include better understanding the role of cascaded quadratic nonlinearities in the formation of the supercontinuum, stabilization of f_{CEO} of the Cr:ZnS oscillators, and power scaling of few-cycle Cr:ZnS lasers and Cr:ZnS-GaSe tandems to tens of Watts [38].

Funding

Office of Naval Research (ONR) grant N00014-15-1-2659; Office of Naval Research (ONR) grant N00014-17-1-2705, Defense Advanced Research Projects Agency (DARPA) grant

Optics EXPRESS

W31P4Q-15-1-0008; Department of Energy (DOE) grant DE-SC0018378; Air Force Office of Scientific Research (AFOSR) grant (FA9550-13-1-0234).

Acknowledgments

A.M. and K.V. acknowledge support from the Office of Naval Research (ONR), grants number N00014-15-1-2659 and N00014-17-1-2705, and from the Defense Advanced Research Projects Agency (DARPA), grant number W31P4Q-15-1-0008. S.M. also acknowledges support from DARPA grant number W31P4Q-15-1-0008, AFOSR grant FA9550-13-1-0234, as well as from the Department of Energy (DOE), grant number DE-SC0018378.

Disclosures

S.M declares competing financial interests.

References

1. Z. Fei, A. S. Rodin, G. O. Andreev, W. Bao, A. S. McLeod, M. Wagner, L. M. Zhang, Z. Zhao, M. Thiemens, G. Dominguez, M. M. Fogler, A. H. Castro Neto, C. N. Lau, F. Keilmann, and D. N. Basov, "Gate-tuning of graphene plasmons revealed by infrared nano-imaging," Nature **487**(7405), 82–85 (2012).
2. F. Huth, A. Govyadinov, S. Amarie, W. Nuansing, F. Keilmann, and R. Hillenbrand, "Nano-FTIR absorption spectroscopy of molecular fingerprints at 20 nm spatial resolution," Nano Lett. **12**(8), 3973–3978 (2012).
3. M. Wagner, A. S. McLeod, S. J. Maddox, Z. Fei, M. Liu, R. D. Averitt, M. M. Fogler, S. R. Bank, F. Keilmann, and D. N. Basov, "Ultrafast dynamics of surface plasmons in InAs by time-resolved infrared nanospectroscopy," Nano Lett. **14**(8), 4529–4534 (2014).
4. H. Timmers, A. Kowligy, A. Lind, F. C. Cruz, N. Nader, M. Silfies, G. Ycas, T. K. Allison, P. G. Schunemann, S. B. Papp, and S. A. Diddams, "Molecular fingerprinting with bright, broadband infrared frequency combs," Optica **5**(6), 727–732 (2018).
5. A. Muraviev, V. Smolski, Z. Loparo, and K. L. Vodopyanov, "Massively parallel sensing of trace molecules and their isotopologues with broadband subharmonic mid-infrared frequency combs," Nat. Photonics **12**(4), 209–214 (2018).
6. A. Wirth, M. Th. Hassan, I. Grguraš, J. Gagnon, A. Moulet, T. T. Luu, S. Pabst, R. Santra, Z. A. Alahmed, A. M. Azzeer, V. S. Yakovlev, V. Pervak, F. Krausz, and E. Goulielmakis, "Synthesized light transients," Science **334**(6053), 195–200 (2011).
7. C. Manzoni, O. D. Mücke, G. Cirmi, S. Fang, J. Moses, S.-W. Huang, K.-H. Hong, G. Cerullo, and F. X. Kärtner, "Coherent pulse synthesis: towards sub-cycle optical waveforms," Laser Photonics Rev. **9**(2), 129–171 (2015).
8. A. I. Adamu, M. S. Habib, C. R. Petersen, J. E. Antonio-Lopez, Bi. Zhou, A. Schülzgen, R. Amezcua-Correa, O. Bang, and C. Markos, "Deep-UV to mid-IR supercontinuum generation driven by mid-IR ultrashort pulses in a gas-filled fiber," Scientific Reports **9**, 4446 (2018).
9. U. Petersen, I. Møller, B. Kubat, S. Zhou, J. Dupont, T. Ramsay, S. Benson, N. Sujecki, A. Moneim, Z. Tang, D. Furniss, A. Seddon, and O. Bang, "Mid-infrared supercontinuum covering the 1.4–13.3 μm molecular fingerprint region using ultra-high NA chalcogenide step-index fibre," Nat. Photonics **8**, 830–834 (2014).
10. Y. Wu, M. Meneghetti, J. Troles, and J. L. Adam, "Chalcogenide microstructured optical fibers for mid-infrared supercontinuum generation: interest, fabrication, and applications," Appl. Sci. (Basel) **8**(9), 1637 (2018).
11. Y. Yu, X. Gai, T. Wang, P. Ma, R. Wang, Z. Yang, D.-Y. Choi, S. Madden, and B. Luther-Davies, "Mid-infrared supercontinuum generation in chalcogenides," Opt. Mater. Express **3**(8), 1075–1086 (2013).
12. Y. Okawachi, M. Yu, J. Cardenas, X. Ji, A. Klenner, M. Lipson, and A. L. Gaeta, "Carrier envelope offset detection via simultaneous supercontinuum and second-harmonic generation in a silicon nitride waveguide," Opt. Lett. **43**(19), 4627–4630 (2018).
13. F. Silva, D. R. Austin, A. Thai, M. Baudisch, M. Hemmer, D. Faccio, A. Couairon, and J. Biegert, "Multi-octave supercontinuum generation from mid-infrared filamentation in a bulk crystal," Nat. Commun. **3**(1), 807 (2012).
14. G. Dubietis, G. Tamošauskas, R. Šuminas, V. Jukna, and A. Couairon, "Ultrafast supercontinuum generation in bulk condensed media," Lith. J. Phys. **57**(3), 113–157 (2017).
15. K. Krupa, A. Labruyère, A. Tonello, B. M. Shalaby, V. Couderc, F. Baronio, and A. B. Aceves, "Polychromatic filament in quadratic media: spatial and spectral shaping of light in crystals," Optica **2**(12), 1058–1064 (2015).
16. B. Zhou and M. Bache, "Multiple-octave spanning mid-IR supercontinuum generation in bulk quadratic nonlinear crystals," arXiv:1603.05804v1 (2016).
17. C. Langrock, M. M. Fejer, I. Hartl, and M. E. Fermann, "Generation of octave-spanning spectra inside reverse-photon-exchanged periodically poled lithium niobate waveguides," Opt. Lett. **32**(17), 2478–2480 (2007).
18. H. Guo, B. Zhou, M. Steinert, F. Setzpfandt, T. Pertsch, H. P. Chung, Y. H. Chen, and M. Bache, "Supercontinuum generation in quadratic nonlinear waveguides without quasi-phase matching," Opt. Lett. **40**(4), 629–632 (2015).

Optics EXPRESS

19. L. A. Ostrovskii, "Self-action of light in crystals," JETP Lett. **5**, 272–275 (1967).
20. R. Desalvo, D. J. Hagan, M. Sheik-Bahae, G. Stegeman, E. W. Van Stryland, and H. Vanherzeele, "Self-focusing and self-defocusing by cascaded second-order effects in KTP," Opt. Lett. **17**(1), 28–30 (1992).
21. A. S. Mayer, C. R. Phillips, and U. Keller, "Watt-level 10-gigahertz solid-state laser enabled by self-defocusing nonlinearities in an aperiodically poled crystal," Nat. Commun. **8**(1), 1673 (2017).
22. R. Šuminas, A. Marcinkevičiūtė, G. Tamošauskas, and A. Dubietis, "Even and odd harmonics-enhanced supercontinuum generation in zinc-blende semiconductors," J. Opt. Soc. Am. B **36**(2), A22–A27 (2019).
23. K. Werner, M. G. Hastings, A. Schweinsberg, B. L. Wilmer, D. Austin, C. M. Wolfe, M. Kolesik, T. R. Ensley, L. Vanderhoef, A. Valenzuela, and E. Chowdhury, "Ultrafast mid-infrared high harmonic and supercontinuum generation with n_2 characterization in zinc selenide," Opt. Express **27**(3), 2867–2885 (2019).
24. S. Vasilyev, I. Moskalev, V. Smolski, J. Peppers, M. Mirov, V. Fedorov, D. Martyshkin, S. Mirov, and V. Gapontsev, "Octave-spanning Cr:ZnS femtosecond laser with intrinsic nonlinear interferometry," Optica **6**(2), 126–127 (2019).
25. S. Vasilyev, I. S. Moskalev, V. O. Smolski, J. M. Peppers, M. Mirov, A. V. Muraviev, P. G. Schunemann, S. B. Mirov, K. L. Vodopyanov, and V. P. Gapontsev, "Super-octave longwave mid-infrared coherent transients produced by optical rectification of few-cycle 2.5-μm pulses," Optica **6**(1), 111–114 (2019).
26. S. Mirov, I. Moskalev, S. Vasilyev, V. Smolski, V. Fedorov, D. Martyshkin, J. Peppers, M. Mirov, A. Dergachev, and V. Gapontsev, "Frontiers of mid-IR lasers based on transition metal doped chalcogenides," IEEE J. Sel. Top. Quantum Electron. **24**(5), 1601829 (2018).
27. S. Vasilyev, I. Moskalev, M. Mirov, V. Smolski, S. Mirov, and V. Gapontsev, "Ultrafast middle-IR lasers and amplifiers based on polycrystalline Cr:ZnS and Cr:ZnSe," Opt. Mater. Express **7**(7), 2636–2650 (2017).
28. S. Vasilyev, I. Moskalev, M. Mirov, V. Smolski, S. Mirov, and V. Gapontsev, "Mid-IR Kerr-lens mode-locked polycrystalline Cr:ZnS and Cr:ZnSe lasers with intracavity frequency conversion via random quasi-phase-matching," Proc. SPIE, **vol. 9731**, Mar. 2016, Art. no. 97310B.
29. K. L. Vodopyanov, "Optical generation of narrow-band terahertz packets in periodically inverted electro-optic crystals: conversion efficiency and optimal laser pulse format," Opt. Express **14**(6), 2263–2276 (2006).
30. A. G. Stepanov, A. A. Mel'nikov, V. O. Kompanets, and S. V. Chekalin, "Spectral modification of femtosecond laser pulses in the process of highly efficient generation of terahertz radiation via optical rectification," JETP Lett. **85**(5), 227–230 (2007).
31. H. R. Telle, G. Steinmeyer, A. E. Dunlop, J. Stenger, D. H. Sutter, and U. Keller, "Carrier-envelope offset phase control: A novel concept for absolute optical frequency measurement and ultrashort pulse generation," Appl. Phys. B **69**(4), 327–332 (1999).
32. T. Fuji, A. Apolonski, and F. Krausz, "Self-stabilization of carrier-envelope offset phase by use of difference-frequency generation," Opt. Lett. **29**(6), 632–634 (2004).
33. T. Fuji, J. Rauschenberger, A. Apolonski, V. S. Yakovlev, G. Tempea, T. Udem, C. Gohle, T. W. Hänsch, W. Lehnert, M. Scherer, and F. Krausz, "Monolithic carrier-envelope phase-stabilization scheme," Opt. Lett. **30**(3), 332–334 (2005).
34. Q. Wang, J. Zhang, A. Kessel, N. Nagl, V. Pervak, O. Pronin, and K. F. Mak, "Broadband mid-infrared coverage (2-17 μm) with few-cycle pulses via cascaded parametric processes," Opt. Lett. **44**(10), 2566–2569 (2019).
35. J. Lind, A. Kowligy, H. Timmers, F. C. Cruz, N. Nader, M. C. Silfies, T. K. Allison, and S. A. Diddams, $\chi^{(2)}$ mid-infrared frequency comb generation and stabilization with few-cycle pulses," arXiv:1811.02604v1 (2018).
36. W. Robert, Boyd, *Nonlinear optics* (Elsevier Academic Press, 2008).
37. S. Kowligy, H. Timmers, A. Lind, U. Elu, F. C. Cruz, P. G. Schunemann, J. Biegert, and S. A. Diddams, "Infrared electric-field sampled frequency comb spectroscopy," arXiv:1808.10275v2 (2018).
38. S. Vasilyev, I. Moskalev, V. Smolski, J. Peppers, M. Mirov, S. Mirov, and V. Gapontsev, "27 Watt middle-IR femtosecond laser system at 2.4 μm," in Laser Congress 2018 (ASSL), OSA Technical Digest (Optical Society of America, 2018), paper AW3A.1.